LABORATORY AND AIRBORNE BRDF ANALYSIS OF VEGETATION LEAVES AND SOIL SAMPLES

Georgi T. Georgiev *Member, IEEE*, Charles K. Gatebe, James J. Butler, Michael D. King, *Senior Member, IEEE*

IEEE Transactions on Geoscience and Remote Sensing

Manuscript received February 29, 2008. This work was supported by the National Aeronautics and Space Administration under Agreement No. NAS5-02041 issued through the Science Mission Directorate.

G. T. Georgiev is with Science Systems and Applications, Inc., Lanham, MD 20706 USA (e-mail: Georgi.T. Georgiev@nasa.gov).

C. K. Gatebe is with the Goddard Earth Sciences and Technology Center, University of Maryland Baltimore County, Baltimore, MD 21228 USA.

J. J. Butler is with Hydrospheric and Biospheric Laboratory, NASA Goddard Space Flight Center, Greenbelt, MD 20771 USA.

M. D. King is with the Earth Sciences Division, NASA Goddard Space Flight Center, Greenbelt, MD 20771 USA.

ABSTRACT

Laboratory-based Bidirectional Reflectance Distribution Function (BRDF) analysis of vegetation leaves, soil, and leaf litter samples is presented. The leaf litter and soil samples, numbered 1 and 2, were obtained from a site located in the savanna biome of South Africa (Skukuza: 25.0°S, 31.5°E). A third soil sample, number 3, was obtained from Etosha Pan, Namibia (19.20^{o}S, 15.93^{o}E, alt. 1100 m). In addition, BRDF of local fresh and dry leaves from tulip tree (*Liriodendron tulipifera*) and acacia tree (*Acacia greggii*) were studied. It is shown how the BRDF depends on the incident and scatter angles, sample size (i.e. crushed versus whole leaf,) soil samples fraction size, sample status (i.e. fresh versus dry leaves), vegetation species (poplar versus acacia), and vegetation's biochemical composition. As a demonstration of the application of the results of this study, airborne BRDF measurements acquired with NASA's Cloud Absorption Radiometer (CAR) over the same general site where the soil and leaf litter samples were obtained are compared to the laboratory results. Good agreement between laboratory and airborne measured BRDF is reported.

***Index Terms*—**BRDF, metrology, optical instrumentation and measurements, remote sensing, vegetation.

I. Introduction

THE monitoring of land surface is a major science objective in Earth remote sensing. A major goal in land remote sensing is to identify major biomes and to map and distinguish the changes in their composition introduced by anthropogenic and climatic factors. Currently, deforestation and desertification are the most important land cover area processes of scientific interest. These processes play a major role in climate variation particularly with respect to clouds and rainfall. Understanding the spatial characteristics of the properties of biomes will help in predicting the changes in major Earth biomes and their impact on climate variation and hence, lead to formulation of better site-specific management plans.

The bidirectional reflectance distribution function (BRDF) describes the reflectance of optical materials as a function of incident and scatter angles and wavelength. It is used in modern optical engineering to characterize the spectral and geometrical optical scatter of both diffuse and specular samples. The BRDF is particularly important in the characterization of reflective and transmissive diffusers used in the pre-flight and on-orbit radiance and reflectance calibration of Earth remote sensing instruments [1]. Satellite BRDF measurements of Earth scenes can be used as a sensitive tool for early detection of changes occurring in vegetation canopies, soils, or the oceans. For example, water content changes in soil and vegetation can be detected and monitored using BRDF.

In this paper, we analyzed laboratory-based BRDF data of vegetation leaves, leaf litter, and soil samples to study, on a small-scale, the effects of spatial and spectral variability in the reflectance of natural biome samples. The samples measured in the laboratory included leaf litter, predominantly from acacia trees, and two different composition regolith soils collected from the savanna biome of Skukuza, South Africa, Fig. 1a. A third soil sample was collected from Etosha Pan, Namibia, Fig. 1b. In addition, BRDF of fresh and dry leaves from tulip tree (*Liriodendron tulipifera*) and acacia tree (*Acacia greggii*) located in Maryland, USA were studied. The laboratory-based BRDF of all samples was analyzed in the principal plane at 340, 470, and 870 nm, at

incident angles of 0° and 67°, and at viewing angles from 0° to 80° for all samples, except the sample from Etosha Pan. The latter has been measured at 412, 555, 667, and 869 nm and at incident angles of 0^o, 30^o and 60^o. BRDF dependence on the sample particle size was investigated by measuring the following three different samples: whole leaves, samples with leaf particle sizes between 4 and 4.75 mm, and samples with leaf particle size between 1.7 and 2 mm. All the BRDF values were measured using NASA Goddard Space Flight Center's (GSFC's) Diffuser Calibration Laboratory (DCL) scatterometer (cf. Fig. 2a). The typical measurement uncertainty was 1% (k = 1) or better, where k is the coverage factor. The results presented are traceable to the National Institute of Standards and Technology's (NIST's) Special Tri-function Automated Reference Reflectometer (STARR).

The DCL has participated in several round-robin measurement campaigns with domestic and foreign calibration institutions in support of Earth and space satellite validation programs [2]. The facility has characterized many types of diffusely reflecting samples including Spectralon, aluminum diffusers, barium sulfate, radiometric tarps, and Martian regolith simulant [4], [5].

The laboratory results were compared to BRDF measurements with an airborne radiometer, Cloud Absorption Radiometer (CAR), which was developed at GSFC (c.f. Fig. 2c) and described by King *et al*. [6]. The CAR is designed to scan from 5° before zenith to 5° past nadir, corresponding to a total scan range of 190°. Each scan of the instrument lies across the line that defines the aircraft track and extends up to 95° on either side of the aircraft horizon. The CAR field of view is 17.5 mrad (1°), the scan rate is 1.67 Hz, the data system has 9 channels at 16 bit and it has 382 pixels in each scan line. CAR's 14 channels are located between 335 and 2344 nm. The CAR channels' exact wavelengths and bandpass widths are shown in Table 1. These bands were selected to avoid atmospheric molecular absorption bands in the near and shortwave infrared. In the normal mode of operation, data are sampled simultaneously and continuously on nine individual detectors. The first 8 data channels between 335 and 1296 nm are always simultaneously and continuously sampled on eight individual detectors, while the ninth data channel is registered for signal selected from the six remaining channels on a filter wheel between 1530 and 2344 nm.

The filter wheel can either cycle through all six wavelengths at a prescribed interval usually changing filters every fifth scan line or lock onto any one of them, mostly 1656, 2103, or 2205 nm, and sample it continuously. Data are collected through the 190° aperture that allows observations of the earth–atmosphere scene around the starboard horizon from local zenith to nadir while the CAR scan mirror rotates 360° in a plane perpendicular to the direction of flight.

In this study, the CAR data were obtained over Skukuza, South Africa (25.0°S, 31.5°E) and Etosha Pan, Namibia (19.20°S, 15.93°E), which are core sites for validation of the Earth Observing System (EOS) Terra satellite instruments. These BRDF measurements are reported in Gatebe *et al.* [3]. A distinct backscattering peak in the principal plane characterizes the BRDF over Skukuza, whereas the BRDF over Etosha pan is more enhanced in the backscattering plane and shows little directional variation.

II. Methodology

The definition and derivation of BRDF are credited to Nicodemus *et al.,* (1977) who presented a unified approach to the specification of reflectance in terms of both incident and reflected light beam geometries for characterizing both diffuse and specular reflecting surfaces of optical materials. He defined the BRDF as a distribution function relating the irradiance incident from one given direction to the reflected radiance in another direction. Thus, the BRDF is presented in radiometric terms as the ratio of the radiance L_r reflected by a surface into the direction (θ_r, ϕ_r) to the incident irradiance, E_i, on a unit surface area from a specified direction (θ_i, ϕ_i) at a particular wavelength, λ, expressed mathematically as:

$$BRDF = \frac{dL_r(\theta_i, \phi_i, \theta_r, \phi_r; E_i)}{dE_i(\theta_i, \phi_i)} \quad (1)$$

where the subscripts *i* and *r* denote incident and reflected light respectively, θ is the zenith angle, and ϕ is the azimuthal angle.

Nicodemus *et al.* [8] further assumed that the incident beam has uniform cross section, the illumination on the sample is isotropic, and all scattering comes from the sample surface and none

from the bulk. The bidirectional reflectance corresponds to directional-directional reflectance and ideally means both incident and reflected light beams are collimated. Although perfect collimation and diffuseness are rarely achieved in practice, they can be used as a very useful approximation for reflectance measurements. In practice, we deal with real sample surfaces that reflect light anisotropically and the optical beams used to measure the reflectance are not perfectly uniform. Hence, from a practical consideration, Stover [11] presented the BRDF in a convenient form for measurement applications. The BRDF is defined in radiometric terms as reflected surface radiance in a given direction divided by the incident surface irradiance from another or the same (i.e. retro) direction. The incident irradiance is the radiant flux incident on the surface. The reflected surface radiance is the light flux reflected through solid angle Ω per projected solid angle:

$$BRDF = \frac{P_r / \Omega}{P_i \cos\theta_r}, \tag{2}$$

where P_r is the reflected radiant power, Ω is the solid angle determined by the area of detector aperture, A, and the radius from the sample to the detector, R. The solid angle can be computed as $\Omega = A/R^2$. P_i is the incident radiant power, and θ_r is the reflected zenith angle. The $\cos\theta_r$ factor is a correction to account for the illuminated area, when viewed from the detector direction. BRDF has units of inverse steradians and can range from very small numbers (e.g. off-specular black samples) to very large values (e.g. highly reflective samples at specular reflectance). Following Stover's concept, the BRDF defining geometry is shown in Fig. 3a, where the subscripts *i* and *r* refer to incident and reflected quantities, respectively. Note that the BRDF is often called cosine-corrected, when the $\cos\theta_r$ factor is not included.

In the case of CAR measurements, the spectral BRDF (R_λ) is expressed following van de Hulst (1980) formulation (see also Fig. 3b):

$$R_\lambda(\theta,\theta_0,\Phi) = \frac{\pi I_\lambda(\theta,\theta_0,\Phi)}{\mu_0 F_\lambda}, \tag{3}$$

where I_λ is the measured reflected intensity (radiance), F_λ is the solar flux density (irradiance) incident on the top of the atmosphere, θ and θ_0 are respectively the viewing and incident zenith angles, Φ is the azimuthal angle between the viewing and incident light directions and $\mu_0 = cos\theta_0$. The R_λ is equivalent to bidirectional reflectance factor (BRF) as defined in Nicodemus et al. [8], which is dimensionless and numerically equivalent to BRDF times π.

The DCL scatterometer was used to measure the BRDF at different wavelengths and at different source and detector angular configurations. Although a more detailed design review on the scatterometer is published by Schiff *et al.,* 1993, we include here some basic information. The scatterometer is located in a class 10000 laminar flow cleanroom. It is capable of measuring the BRDF and BTDF of a wide range of samples including white and gray-scale diffusers, black painted or anodized diffusers, polished or roughened metal surfaces, clean or contaminated mirrors, transmissive diffusers, liquids, and granular solids. The operational spectral range of the instrument is from 230 to 900 nm. The scatterometer can perform in the principal plane and out-of the principal plane BRDF measurements. It consists of a vertical optical source table, a sample stage, a detector goniometer, and a computer system for positioning control, data collection and analysis.

The optical table can be rotated around its horizontal axis located at the table center to change the incident angle, θ_i, relative to the sample normal (cf. Fig.2a). The optical source table contains two light sources—a 75 W xenon short-arc lamp coupled to a Chromex 250SM scanning monochromator and a replaceable coherent source in the operational spectral range. The scattered light from the sample is collected using an ultraviolet-enhanced silicon photodiode detector with output fed to a computer-controlled lock-in amplifier. The sample is mounted on a sample stage in the horizontal plane. The sample stage allows proper positioning of the sample with respect to the incident beam. It can be moved in X, Y and Z linear directions using three motors. The sample stage provides sample rotation in the horizontal plane around the Z axis, thereby enabling changes in the incident azimuthal angle, ϕ_i. The standard scatterometer sample stage can accommodate samples as large as 45 cm square and up to 4.5 kg in weight. However,

larger samples have been measured using custom designed sample adapters. As shown in Fig. 2a, the detector assembly moves along the arc providing the ability to make reflectance measurements as a function of the viewing zenith angle, θ_r. The arc rotates 180° around the vertical Z axis which determines the viewing azimuthal angle, ϕ_r. The center of the illuminated spot on the surface of the sample has to be positioned at the cross point of the three perpendicular goniometer rotation axes, X, Y, Z, coinciding with the center of a sphere with radius equal to the distance between that point and the detector assembly's cover aperture.

The illuminated area on the sample underfills the FOV of the measurement detector. All measurements in the current study were made for polarizations of the incident beam parallel, *P*, and perpendicular, *S*, to the plane of incidence. The BRDF for each polarization was calculated by dividing the net signal from the reflected radiant flux by the incident flux and the projected solid angle from the calibration item to the limiting aperture of the detector. The BRDF values for both polarizations were then averaged to yield the BRDF for unpolarized incident radiant flux and the values of the unpolarized scattering case are reported in this paper. The operation of the scatterometer is fully computerized. Customized software controls all motion, data acquisition and data analysis.

III. MEASUREMENTS

For the study described in this paper, we studied vegetative and soil samples from 3 different locations. The first location was Skukuza, South Africa, the second Etosha Pan, Namibia, and the third Maryland, USA.

Skukuza (see Fig. 1a) is a well foliaged rest camp on the southern banks of Sabie River in southern in Kruger National Park. The site exhibits typical savanna ecosystem characteristics: more-or-less continuous vegetation cover with trees and shrubs in varying proportions. The differences in the composition, structure and density of plant communities are attributable to the influence of the moisture in the area, as well as differences in the terrain: altitude and slope, as well as soil type and the prevalence of fires. The environment and vegetation of the flux meas-

urement site near Skukuza is best described by Scholes *et al.* [10]. The vegetation is dominated by savanna grass and knob thorn trees (*Acacia nigrescens*) with their flat, relatively narrow crown and sparse canopy. They grow 5 to 18 m in height, are fire-resistant, and are eaten by giraffes and other animals. The leadwood (*Combretum imberbe*) is also common. It normally grows up to 20 m, has a spreading, rather sparse, roundish to slightly umbrella-shaped crown, and a single, thick trunk.

The Skukuza samples shown in Fig. 4a were a <2 mm diameter fraction of soil and dry leaf litter. The leaf litter is predominantly from acacia trees and savanna grass. The soil sample S1 is a coarse loamy-sand soil with dominant grass roots from the top of the organic horizon, layer depth of 0–30 cm. The soil sample S2 is an exposed coarse loamy-sand soil from the mineral horizon, layer depth 30–40 cm.

The Etosha Pan (see Fig. 1b) is 4590 square kilometers in area and 120 x 72 km in extent situated in northern Namibia. It is desert like, white in color, and dry salt pan without any vegetation. During rainy years, however, Etosha pan becomes approximately a 10 cm deep lake and becomes a breeding ground for thousands of flamingos. Etosha Pan has unique reflective characteristics. It's reflectance spectra is high in the blue, around 440 nm. This explains the apparent white color of the pan as brighter objects in the blue part of the visible spectrum appear whiter to the human eye. The Etosha Pan mineralogy is dominated by four compounds, (i) feldspar and mica, (ii) feldspar and sepiolite, (iii) silicates, and (iv) calcite and dolomite which determine the pan's reflectance spectra. The Etosha pan surroundings are dominated by mopane and acacia trees and grasslands. We studied four different Etosha Pan soil samples (see Fig. 4b). The first Etosha sample, named here as "the rock", is a solid piece of pan sediment, while the other three samples are regoliths with fractional sizes of 0.5 mm or less for Etosha Pan sample 1 hereafter EP1, between 1 and 2 mm for EP2, and a sub millimeter fraction for EP3.

In addition to Skukuza and Etosha Pan, samples from Maryland, USA consisting of whole and crushed, fresh and dried acacia and poplar tree leaves were studied, as shown in Figs. 4c and d. All samples were air dry at the time of this study except the fresh acacia and poplar samples.

The samples were placed in square 50 × 50 × 5 mm black plastic holders with the sample surfaces well flattened. Care was taken for uniform particle distribution through the entire surface area. The holders were mounted horizontally on the sample stage and aligned with the scatterometer axes of rotation.

The laboratory study of Skukuza samples was done at the same wavelengths, incident and view angles as the CAR instrument airborne measurements over Skukuza. The incident angles for the Skukuza samples were 0° and 67°, the zenith view angles were from 0° to 80° with data acquired in steps of 5°, the azimuthal angles were 0° and 180° corresponding to the principal plane measurement geometry. The measurement wavelengths were 340, 470, and 870 nm, again based on CAR operating wavelengths. The top and bottom of the leaves were measured to account for structural differences such as smoothness and glossiness.

Similarly, Etosha Pan samples were studied at wavelengths, incident and view angles comparable to the airborne measurements over Etosha Pan. The Etosha Pan samples were characterized in the DCL at incident angles of 0°, 30° and 60° and zenith view angles from 0° to 80° in steps of 5°. The DCL measurement wavelengths were 412 nm, 555 nm, 667 nm, and 869 nm. However, only 667 nm and 869 nm correspond to the CAR's operational wavelengths.

The CAR instrument was flown aboard the University of Washington Convair CV-580 research aircraft during the Southern Africa Regional Science Initiative 2000 (SAFARI 2000) dry season campaign. The airborne CAR data from a vegetation rich surface was recorded over Skukuza during the dry season in August 2000 for view angles from –80° to 80° and at a number of wavelengths. The BRDF of the savanna surface was acquired at 67° incident angle and viewing angles from -80^{o} to 80^{o} in 8 spectral bands from 0.34 to 1.27 μm. A hot spot or retroscatter signal was seen at about -70^{o}. The airborne computed BRDF shows backscattering properties of the vegetation covered soil surface.

IV. Results and Discussion

A. Laboratory-based BRDF of Savanna Samples, Skukuza

The laboratory-based BRDF at normal incidence for the two soils, S1 and S2, and a savanna leaf litter sample is shown in Fig. 5a at 870 nm. The BRDF at 340 and 470 nm is not shown in this paper as the spatial distribution is similar for those wavelengths. In addition to BRDF measurements, the samples' spectral reflectance was measured with an Analytical Spectral Device (ASD) spectroradiometer in-plane at 0° incident angle and 60° viewing angle from 350 to 2500 nm. The results are compared in Fig. 5b, where the reflectance spectrum for fresh acacia leaf taken at the same measurement geometry is also included. The leaves' complex biochemical composition made up of chlorophyll, pigments, proteins, starches, waxes, water, lignin, and cellulose is apparent in their reflectance spectra. The chlorophyll and pigments influence the spectra in the visible region. The water content and leaf structure contribute to the reflectance in the near-infrared, while the proteins, lignin and cellulose contribute in the shortwave-infrared, Kokaly *et al*. [7]

The difference in BRDF of dry and fresh acacia and poplar tree leaves at normal incidence is shown in Fig. 6a at 340 nm, and in Fig. 6b at 470 nm. The overall reflectance of the acacia dry leaves is higher at all wavelengths. However, the fresh poplar leaves have a higher BRDF in the backscattering direction. Both fresh and dry poplar leaves have higher BRDF than the acacia leaves at smaller scatter zenith angles (i.e. 0° to 30°) and lower BRDF at larger scatter zenith angles (i.e. 30° to 80°). The difference in BRDF between the two species illustrates the importance of accurate identification of the types of vegetation in airborne data recording. The difference is higher at scatter zenith angles from 5° to 45° and decreases at larger angles. However, the percent difference of the BRDF varies between 20% and 60% depending on the wavelength. The data at 340 and 470 nm are in the spectral region where mainly pigments dominate the leaf reflectance, whereas the BRDF at 870 nm is affected largely by the water content and leaf structure. For all leaves, there is also a difference in BRDF between the top and bottom sides of the leaves. On average the bottom BRDF of the acacia was always higher: 34% at 340 nm, 48% at

470 nm, and 4% at 870 nm due to the leaves' surface structure.

The BRDF of cut leaves was also measured to address scaling issues in the remote sensing of vegetation. It was estimated that for airborne BRDF measurements of land surfaces from a 600 m altitude, the footprint of a typical savanna tree would correspond to a leaf particle size in the laboratory of ~ 4 mm, whereas the footprint of a typical savanna bush would correspond to a size of ~ 2 mm. We compared the BRDF of a whole leaf to that of leaves crushed to 2 and 4 mm sizes. The BRDFs of crushed and whole fresh samples of poplar leaves at 340 nm are shown in Fig. 7a at normal incidence.

There is a significant difference between the measured BRDFs of whole and crushed leaves at small viewing angles from 5° to 45°. The percent differences between the BRDF of whole leaves and crushed leaves having a 4 mm particles size are up to 55% at 5° viewing angle and up to 59% for the 2 mm sample. The differences at scatter angles from 45° to 80° are on the order of 27% at 80° viewing angle for whole leaves versus 4 mm crushed leaves and 18% for whole leaves versus 2 mm crushed leaves. The possible explanation for this is that the scatter from the whole leaf has a strong specular component leading to higher reflectance at small scatter angles. The scatter from the crushed leaves is more diffuse resulting in much lower BRDF at small angles. The second reason for the different BRDF is the shadowing effect that takes place when the surface of a sample is not flat but consists of small particles. In the crushed leaf BRDF sample the scattering between the individual leaf particles is a significant contributor to the reflected distribution of scattered light. The BRDF of the 4 mm sample is higher than the BRDF of the 2 mm sample because the smaller particles exhibit more extensive shadowing. However, the difference in the BRDF of 2 mm and 4 mm samples is relatively small and is not a strong function of increasing scatter angle. We observed the same BRDF relation at other wavelengths as well.

Whole, 2 mm, and 4 mm poplar leaves were measured at an incident angle of 67° as shown in Fig. 7b, which shows data acquired at 870 nm. For non-normal illumination geometries, the leaves exhibit strong forward scattering at all wavelengths for both fresh and dry samples. The

backscattering is stronger for the dry samples. The BRDF of fresh and dry poplar leaves at 67^o incident angle were compared at 340, 470, and 870 nm. The BRDF is lower at shorter wavelengths; however, the scattered light spatial distribution pattern is largely independent of wavelength. The glossy surface of a whole leaf has a well-pronounced specular component, whereas the crushed samples show predominantly diffuse scattering. The shadowing effect of the sample particles is also evident at 67° incident angle.

The soil and leaf litter samples' BRDF are shown in Fig. 8 at 340 nm and 870 nm. The BRDF distribution depends strongly on the nature of the sample (i.e., soil versus leaf) and the viewing angle. The soil samples, S1 and S2, exhibit enhanced optical backscattering. The leaf litter sample, L, however, behaves differently. The L sample exhibits equal forward scattering at 340 nm as seen in Fig. 8a and enhanced backscattering at 470 and 870 nm, Fig. 8b, (470 nm data is not shown). The enhanced backscattering in the L sample is seen to increase with increasing wavelength. Although the BRDF at $\theta_i = \theta_s$ could not be measured due to the relative geometries of the scatterometer source optics and detector, the BRDF for all samples show evidence of a significant opposition effect represented by increased light being retroscattered back in the direction of the incident beam.

In order to compare the laboratory-based BRDF with the airborne measurements, we calculated a composite laboratory-based BRDF from the following laboratory measured BRDF of four different samples: fresh and dry acacia leaves, crushed leaf litter, and soil samples. The ratio of each sample used to produce the composite laboratory-based BRDF was determined by the distribution of the four components as seen by the CAR instrument during its airborne missions. From a careful examination of photographs taken over Skukuza during SAFARI 2000, we estimated that the vegetation cover was 90% (80% fresh, 10% dry), 5% exposed leaf litter, and 5% exposed soil. The vegetation includes tree canopies as well as savanna grass. The simulated scene BRDF from the fractional laboratory-based BRDF measurements and CAR airborne data are presented in Fig. 9.

The same general shape of the BRDF of the laboratory-measured samples and airborne

measurements can be seen in the data of Fig 9. The BRDF matches very well from 0° to 60° viewing angle at 470 nm and from -15° to 60° viewing angle at 870 nm. However, there is a significant deviation between the laboratory and airborne data at increasingly negative scatter angles, corresponding to backscatter directions. The identification of the sources of differences in laboratory and airborne BRDF measurements through quantification of their effects on measured BRDF is an on-going goal of this research.

B. Laboratory-based BRDF of salt pans, Etosha Pan

The laboratory-based BRDF at 30^o incidence for the four Etosha Pan samples is shown in Fig. 10 at 667 nm. The rock sample's BRDF is higher as the particulate incident light shadowing and scatter light obscuration effects are the smallest. The finest structure sample, No.1 has distinctively higher BRDF than the two other larger fractions, samples No. 2 and 3. It is worth noting that the shape of the BRDF curve for the rock sample is different than the shape of the regolith samples. It is also very important that all samples have apparent backscattering properties. Although the BRDF at $\theta_i = \theta_s$ could not be measured due to the relative geometries of the scatterometer source optics and detector, the BRDF for all samples shows evidence of a significant opposition effect represented by increased light being retroscattered back in the direction of the incident beam. Sample No.2, with particle sizes between 1 and 2 mm, has the lowest BRDF. In addition to BRDF measurements, the samples' spectral reflectance was measured with an Analytical Spectral Device (ASD) spectroradiometer in-plane at 30° incident angle and 30° angle from 350 to 2500 nm (see Fig. 11). The ASD reflectance spectra presents a full reflectance picture for the VIS-NIR spectral range providing additional information on the Etosha Pan sample's reflectance properties.

In order to correctly compare the laboratory-based BRDF with the airborne measurements, we calculated the composite laboratory-based BRDF from the laboratory measured BRDF of the three different Etosha Pan samples. The ratio of each sample in the calculated laboratory-based BRDF was determined by the distribution of the three components as seen by the CAR instru-

ment during the airborne measurements. From a careful examination of photographs of Etosha Pan the components were determined to be 25% EP1, 50% EP2, and 25% EP3. The simulated fractional laboratory-based data is compared to the CAR airborne data in Fig. 12.

The same general shape of the laboratory-measured samples and airborne measurements can be seen in Fig. 12. The data matches well into the uncertainty for both wavelengths all over the viewing angular range with the exception of -80^{o} where the CAR measured data are slightly higher. However, the airborne data at those two wavelengths are very close. The laboratory based data at 667 and 869 nm do show a larger difference than the CAR data at those wavelengths.

V. Conclusions

This work is intended to describe more completely the BRDF of savanna vegetation and soil samples from Skukuza and soil samples from Etosha Pan measured in a laboratory environment. In addition, the laboratory results are compared to in-situ measurements of these areas by the CAR instrument. In the laboratory measurements, the BRDF depends on the incident and viewing angles, on the nature of the sample (i.e., crushed versus whole leaf), on the sample status (fresh versus dry), on the sample biochemical composition for Skukuza samples, and on the particle size fraction for Etosha Pan samples. The analysis shows strong spectral dependence of the BRDF data on the leaf biochemical composition. The BRDF of the acacia whole leaf bottom was always higher than the BRDF of the top of the same leaf, due to the surface physical structure. The difference in BRDF between the two plant species, acacia and poplar, can be as high as 100%, illustrating the importance of knowing the vegetation type for airborne measurements. The difference between the BRDF of whole leaves, 4 mm, and 2 mm crushed leaves can be as high as 55% at 5° scatter zenith angle due to a strong specular component for the whole leaf sample and the presence of incident light shadowing and scattered light obscuration for the crushed leaves samples. The laboratory-based BRDF of Etosha Pan samples depend on sample fraction. It is highest for the rock sample and lowest for the larger size particles regolith sample.

Laboratory-based and CAR airborne data sets were compared at 470 and 870 nm for Skukuza. They matched very well from 0° to 60° viewing angle at 470 nm and from -15° to 60° viewing angle at 870 nm. However, there is a discrepancy between the laboratory and airborne data at negative viewing angles, particularly at higher angles. We examined the difference between the optical scattering properties of fresh and dried vegetation in an effort to identify possible source for this difference. The degree of senescence of vegetation is one potential source for this difference. Laboratory-based and CAR airborne data sets from Etosha Pan were compared at 682 and 870 nm for the airborne data and 677 and 869 nm for the laboratory data, respectively. The BRDF curves have the same general shape, and the data matches well into the uncertainty for both wavelengths over all viewing angular range. However, the airborne data show smaller BRDF differences between the two wavelengths than the laboratory-based data. The effects of atmospheric absorption and scattering from CAR measurements could be a source of uncertainty. We believe the laboratory results are going to be of great use to the remote sensing community in their modeling and correction efforts of airborne data.

REFERENCES

[1] Butler, J. J., B. C. Johnson, and R. A. Barnes, "The calibration and characterization of Earth remote sensing and environmental monitoring instruments," in *Optical Radiometry*, A. C. Parr, R. U. Datla, and J. L. Gardner, Eds., New York: Academic Press, pp. 453-534, 2005.

[2] Early, E. A., P. Y. Barnes, B. C. Johnson, J. J. Butler, C. J. Bruegge, S. F. Biggar, P. S. Spyak, and M. M. Pavlov, "Bidirectional reflectance round-robin in support of the Earth observing system program," *J. Atmos. Oceanic Technol.*, vol. 17, pp. 1077-1091, 2000.

[3] Gatebe, C. K., M. D. King, S. Platnick, G. T. Arnold, E. F. Vermote, and B. Schmid, "Airborne spectral measurements of surface-atmosphere anisotropy for several surfaces and ecosystems over southern Africa," *J. Geophys. Res.*, vol. 108, 8489, doi:10.1029/2002JD002397, 2003.

[4] Georgiev, G. T., and J. J. Butler, "Bidirectional reflectance distribution function and directional-hemispherical reflectance of a Martian regolith simulant," *Opt. Eng.*, vol. 44, no. 036202, 2005.

[5] Georgiev, G. T., and J. J. Butler: "Long-term calibration monitoring of spectralon diffusers BRDF in the air-ultraviolet", *Appl. Opt.*, vol. 46, no. 32, pp. 7892-7899, 2007.

[6] King, M. D., M. G. Strange, P. Leone, and L. R. Blaine, "Multiwavelength scanning radiometer for airborne measurements of scattered radiation within clouds," *J. Atmos. Oceanic Technol.*, vol. 3, pp. 513-522, 1986.

[7] Kokaly, R. F., and R. N. Clark, "Spectroscopic determination of leaf biochemistry using band-depth analysis of absorption features and stepwise multiple regression," *Remote Sens. Environ*., vol. 67, pp. 267-287, 1999.

[8] Nicodemus, F. E., J. C. Richmond, J. J. Hsia, I. W. Ginsburg, and T. Limperis, "Geometrical considerations and nomenclature for reflectance," *National Bureau of Standards (NBS) monograph 160*, 1977.

[9] Schiff, T. F., M. W. Knighton, D. J. Wilson, F. M. Cady, J. C. Stover, and J. J. Butler, "Design review of a high accuracy UV to near infrared scatterometer," *Proc. SPIE*, vol. 1993,

pp. 121-130, 1995.

[10] Scholes, R. J., N. Gureja, M. Giannecchinni, D. Dovie, B. Wilson, N. Davidson, K. Piggott, C. McLoughlin, K. van der Velde, A Freeman, S. Bradley, R. Smart, and S. Ndala, "The environment and vegetation of the flux measurement site near Skukuza, Kruger National Park," *Koedoe,* vol. 44, no. 1, pp. 73–83, 2001.

[11] Stover, J. C., "Optical scattering: Measurement and analysis," *SPIE Press*, Bellingham, Washington, 1995.

[12] van de Hulst, H. C., *Multiple light scattering, Tables, Formulas, and Applications*, vol. 1. San Diego: Academic Press, 1980.

Georgi T. Georgiev (M'07) received his Diploma in engineering from the Budapest Technical University, Budapest, Hungary. He received Ph.D. in physics from the Bulgarian Academy of Sciences, Sofia, Bulgaria in 1998. He has been a research scientist with the Central Laboratory of Mineralogy and Crystallography, Bulgarian Academy of Sciences. He was associated for two years with the University of Maryland, where he worked on NASA's Goddard Space Flight Center projects on acousto-optic imaging spectroscopy for space applications. He is currently with Science Systems and Applications, Inc., and the Calibration Facility of NASA's Goddard Space Flight Center, Greenbelt, Maryland.

His research interests are in the fields of optical scattering and diffraction, and acousto-optics. He is involved in instrument development and measurements of bidirectional scattering distribution functions (BSDFs) in the ultraviolet through shortwave-infrared wavelength regions on a variety of optical and non-optical materials. His publications reflect research interests in optical scattering and acousto-optic devices. He is a member of SPIE, IEEE and the Optical Society of America.

Charles K. Gatebe received the B.Sc. (meteorology, mathematics, and physics) and M.Sc. (meteorology) degrees from the University of Nairobi, Kenya, in 1990 and 1994, respectively, and the Ph.D. degree in atmospheric sciences from the University of the Witwatersrand, South Africa, in 1999. He taught courses on air pollution using nuclear related techniques at the Institute of Nuclear Science, University of Nairobi from 1995–1998 and came to NASA Goddard Space Flight Center (GSFC) in 1999 as a Resident Research Associate of the Universities Space Research Association (USRA). He is currently an associate research scientist in the Goddard Earth Science and Technology Center, University of Maryland Baltimore County based at GSFC. Dr Gatebe is interested in airborne measurements of BRDF over different types of surfaces to elaborate important surface and atmosphere radiative transfer functions and improve remote sensing retrievals of aerosols and clouds. Dr. Gatebe received the World Meteorological Organization Young Scientist Award in 2000 and was honored in 2008 by NASA GSFC's Climate and Radia-

tion Branch for his outstanding scientific leadership in conducting airborne measurements.

James J. Butler received the B.S. degree in physical chemistry from the University of Notre Dame, Notre Dame, IN, in 1977, and the Ph.D. degree in physical chemistry from the University of North Carolina, Chapel Hill, in 1982. He is an optical physicist in the Hydrospheric and Biospheric Sciences Laboratory at NASA's Goddard Space Flight Center (GSFC), where he has been a research scientist since 1984. Since January 1995 and January 2003, he has performed the duties of EOS calibration scientist and NASA's representative to the NPOESS Joint Agency Requirements Group (JARG), respectively. Since June 2004, he has also served as NASA's deputy project scientist for instruments and calibration within the NPOESS Preparatory Project (NPP). He also manages the NASA/GSFC diffuser calibration facility. His previous research experience at NASA includes ground-based and balloon-borne lidar for the detection of stratospheric molecular and radical species, and laser-induced fluorescence of molecules and radicals.

Michael D. King (M'01–SM'03) received the B.A. degree in physics from Colorado College, Colorado Springs, in 1971, and the M.S. and Ph.D. degrees in atmospheric sciences from the University of Arizona, Tucson, in 1973 and 1977, respectively.

In January 1978 he joined NASA Goddard Space Flight Center, Greenbelt, MD, and is currently Senior Project Scientist of NASA's Earth Observing System (EOS), a position he has held since 1992. He is a member of the MODIS Science Team where he has primary responsibility for developing the cloud optical and microphysical property and Level-3 algorithms. His research experience includes conceiving, developing, and operating multispectral scanning radiometers from a number of aircraft platforms in field experiments ranging from arctic stratus clouds to smoke from the Kuwait oil fires in the Persian Gulf and biomass burning in Brazil and southern Africa.

Dr. King is a Fellow of the American Geophysical Union (AGU) and the American Meteorological Society (AMS), and a member of the U.S. National Academy of Engineering. He received the AMS Verner E. Suomi Award for significant and fundamental contributions to remote

sensing and radiative transfer, and the IEEE Prize Paper Award.

TABLE I

CAR SPECTRAL CHANNELS

8 Continuously Sampled Channels		6 Filter Wheel Channels	
Spectral Channel	Wavelength (FWHM) (nm)	Spectral Channel	Wavelength (FWHM) (nm)
1	340 (9)	9	1556 (32)
2	381 (6)	10	1656 (45)
3	472 (21)	11	1737 (40)
4	682 (22)	12	2103 (44)
5	870 (22)	13	2205 (42)
6	1036 (22)	14	2302 (43)
7	1219 (22)		
8	1273 (23)		

FIGURE CAPTIONS

Fig. 1. a) Skukuza, b) Etosha Pan.

Fig. 2. a) Scatterometer goniometric part, b) Scatterometer optical setup, c) CAR instrument.

Fig. 3. Angular conventions: a) BRDF, b) BRF.

Fig. 4. Skukuza leaf litter (L) and soil samples (S1) and (S2), b) Etosha Pan samples EP1, EP2, and EP3, c) Fresh acacia and dry poplar tree leaves and d) 2 mm and 4 mm cut poplar tree leaves.

Fig. 5. a) Laboratory-based BRDF of S1, S2 and L samples at normal incidence and 870 nm. b) ASD reflectance spectra of leaf litter, soil and cut leaves.

Fig. 6. a) Laboratory-based BRDF of acacia and poplar trees dry and fresh leaves at normal incidence and: a) 340 nm, b) 470 nm.

Fig. 7. BRDF of whole, 4 mm, and 2 mm cut poplar leaves at a) normal incidence and 340 nm. b) 67° incidence and 870 nm.

Fig. 8. BRDF of soil and leaf litter at 60° and a) 340 nm, b) 870 nm.

Fig. 9. Simulated scene BRDF from the fractional laboratory-based BRDF measurements and CAR airborne data at 470 and 870 nm.

Fig. 10. BRDF of Etosha Pan samples at 30^{o} incident angle and 667 nm.

Fig. 11. ASD reflectance of Etosha Pan samples at 30^{o} incident angle and 30^{o} scatter zenith angle.

Fig. 12. Etosha Pan simulated scene BRDF from the fractional laboratory-based BRDF and CAR airborne data.

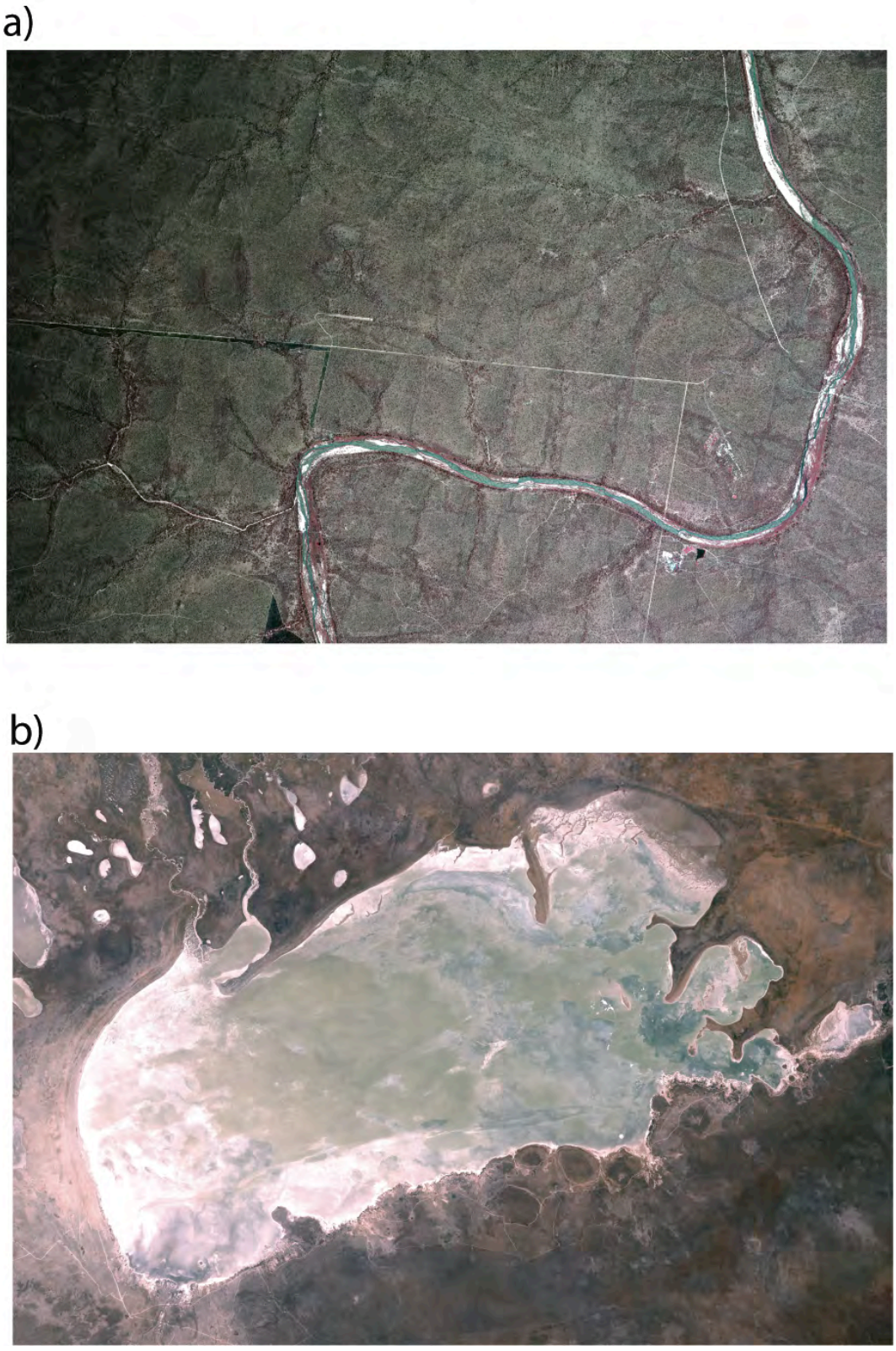

Fig. 1: a) Skukuza, b) Etosha Pan

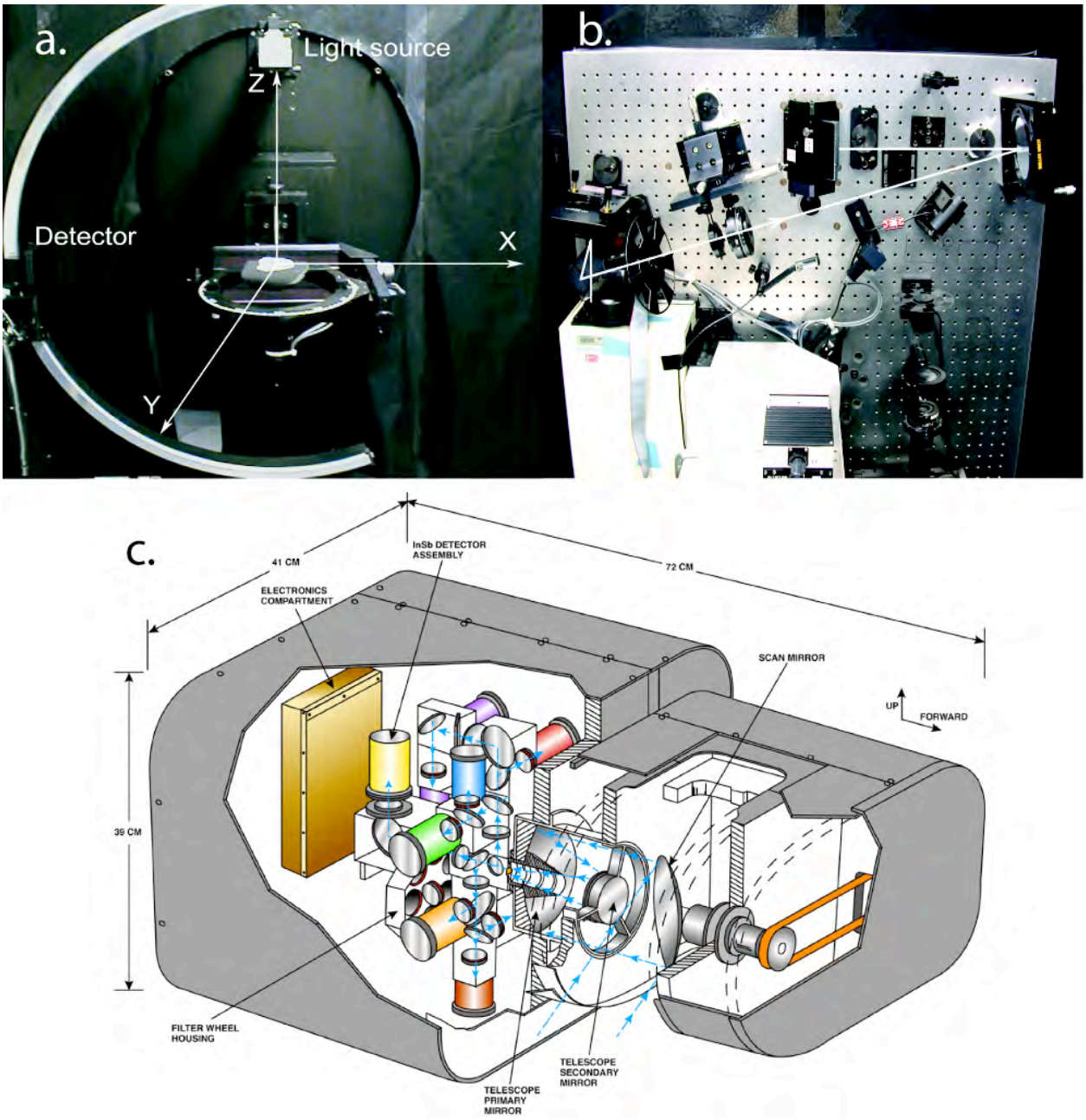

Fig. 2: a) Scatterometer goniometric part, b) Scatterometer optical setup, c) CAR instrument

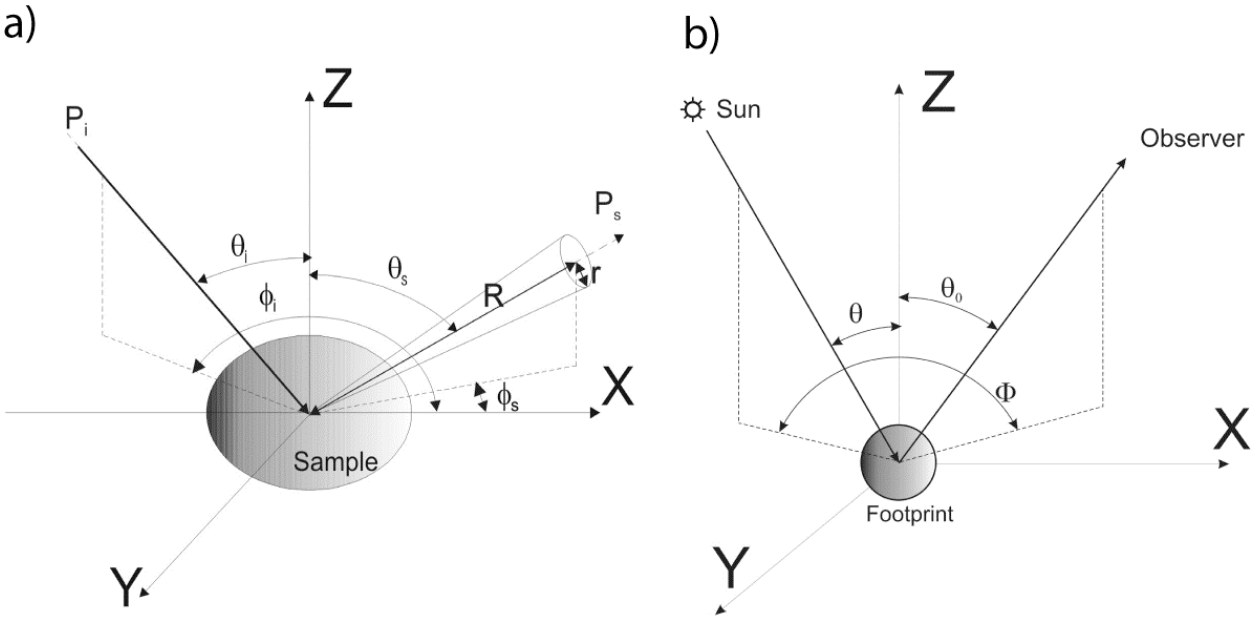

Fig. 3: Angular conventions: a) BRDF, b) BRF.

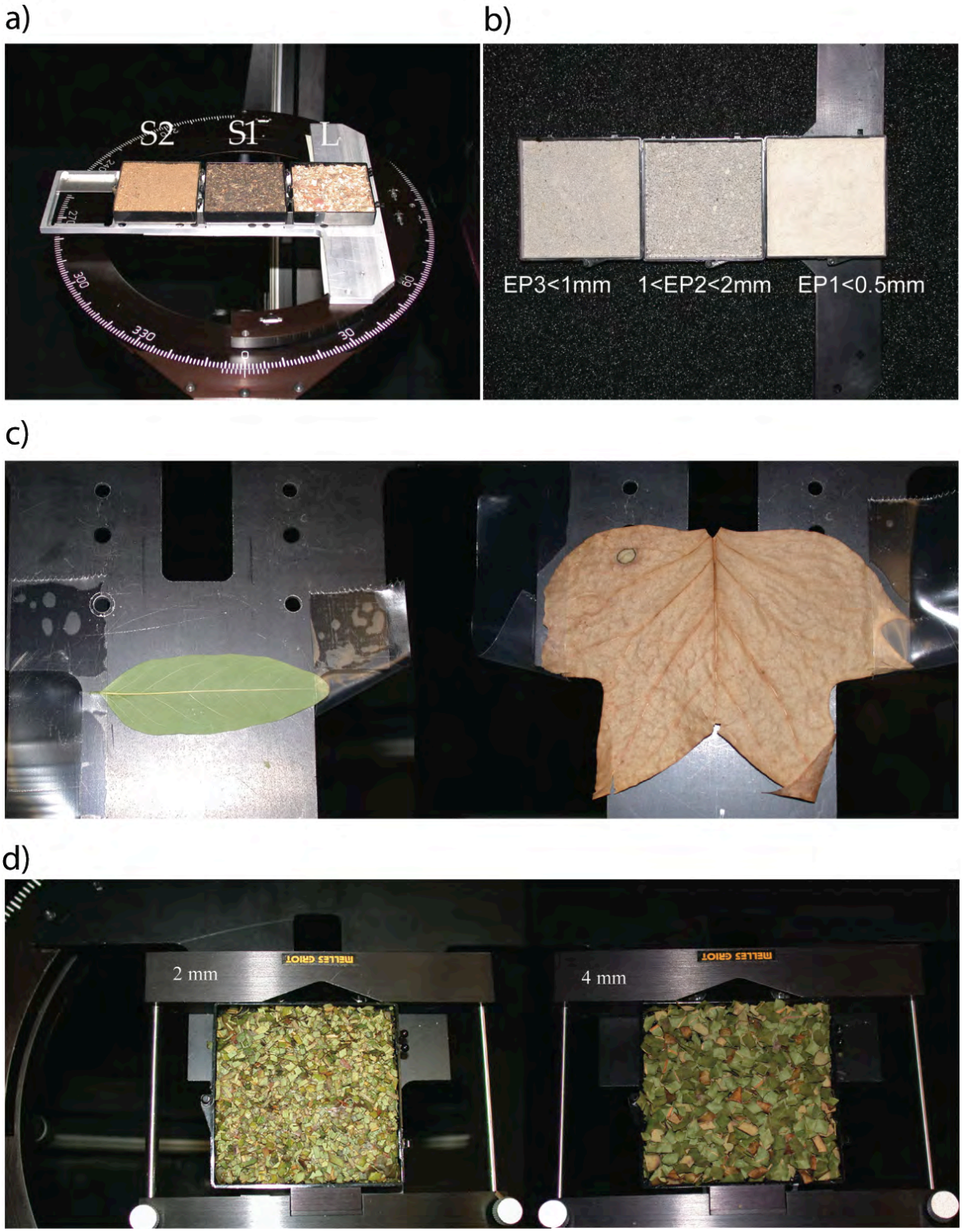

Fig. 4: a) The leaf litter (L) and soil samples (S1) and (S2), b) Etosha Pan samples, c) Fresh acacia and dry poplar tree leaves and d) 2 mm and 4 mm cut poplar tree leaves.

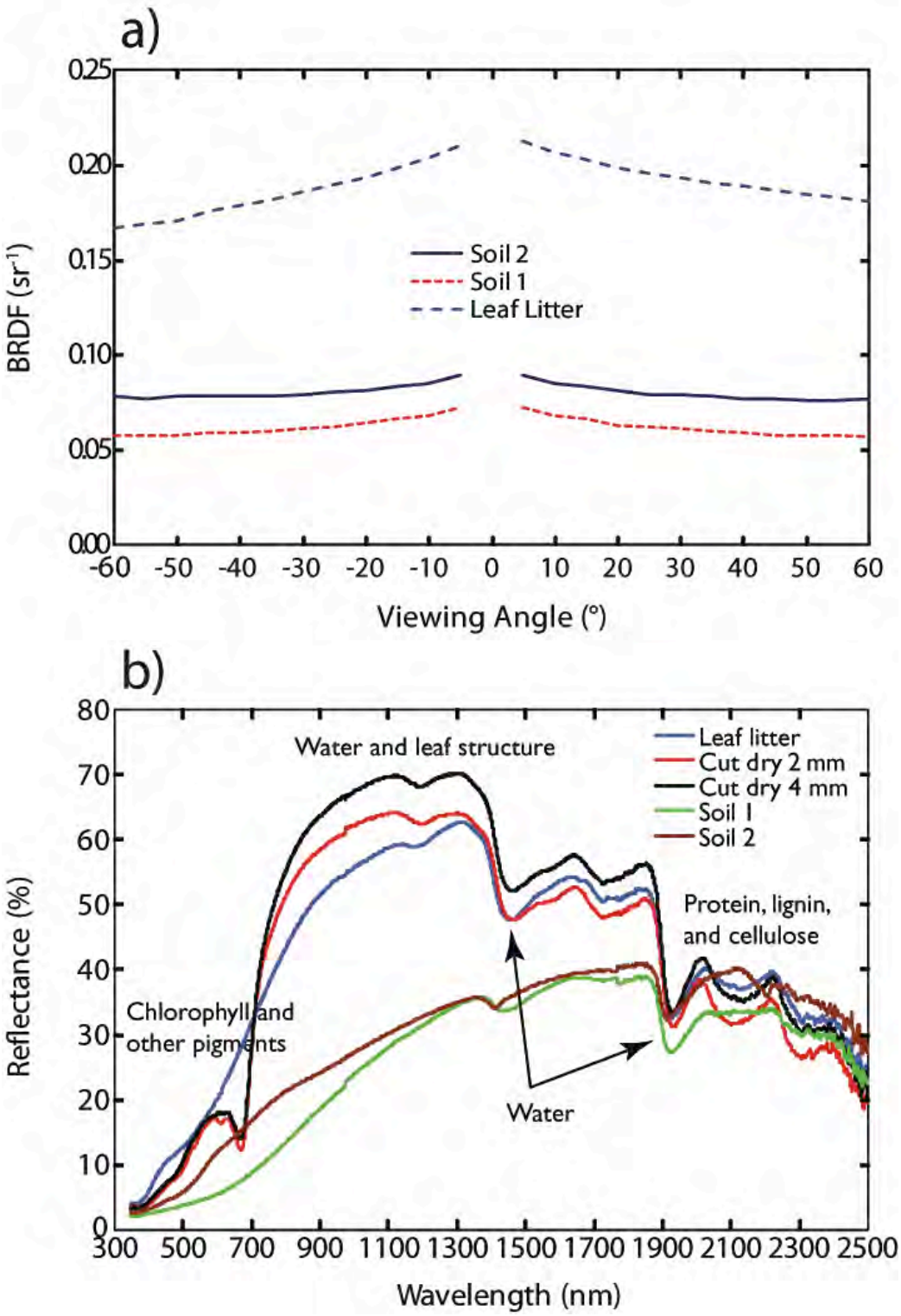

Fig. 5. a) Laboratory-based BRDF of S1, S2 and L samples at normal incidence and 870 nm. b) ASD reflectance spectra of leaf litter, soil and cut leaves.

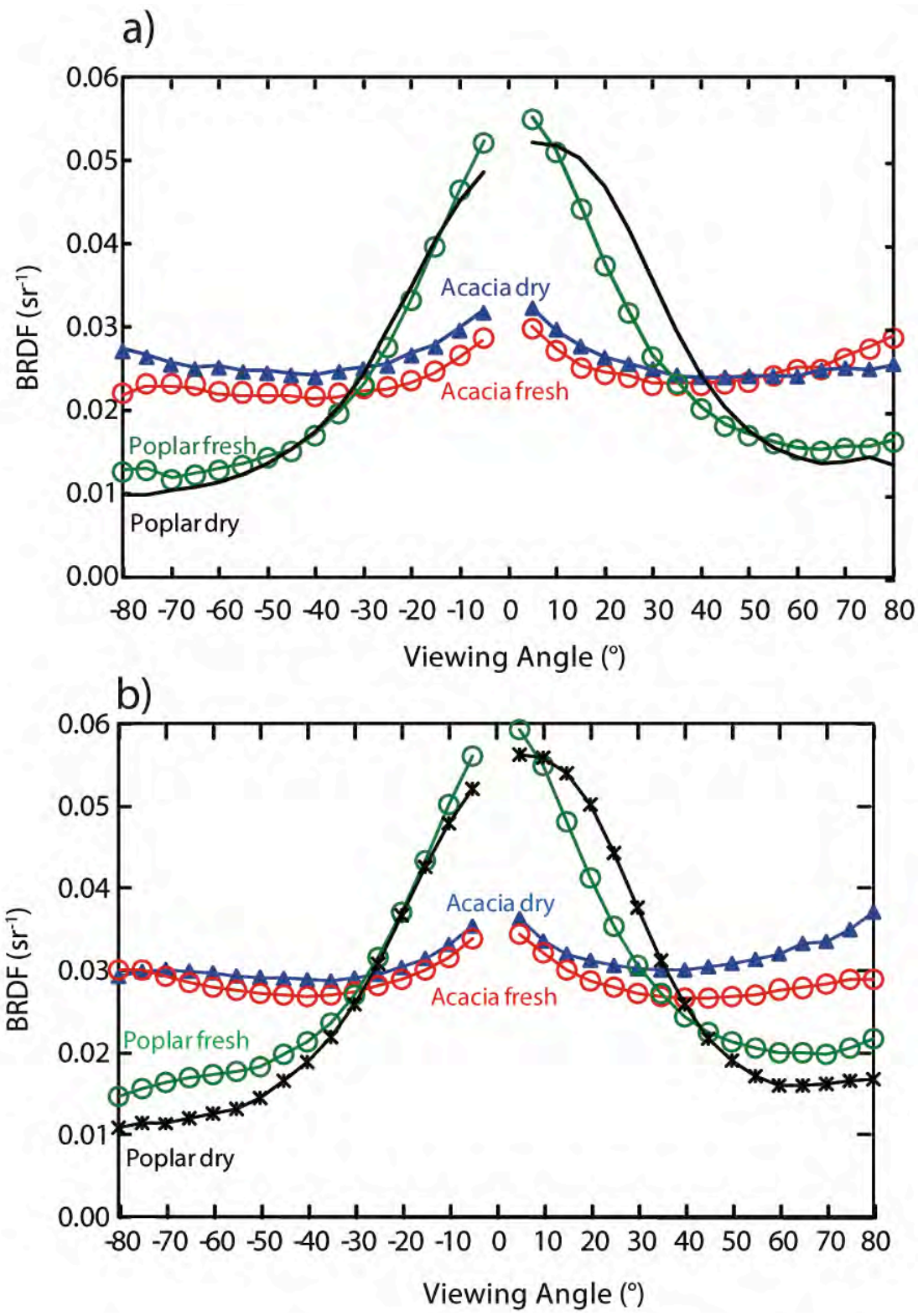

Fig. 6. a) Laboratory-based BRDF of acacia and poplar trees dry and fresh leaves at normal incidence and: a) 340 nm, b) 470 nm.

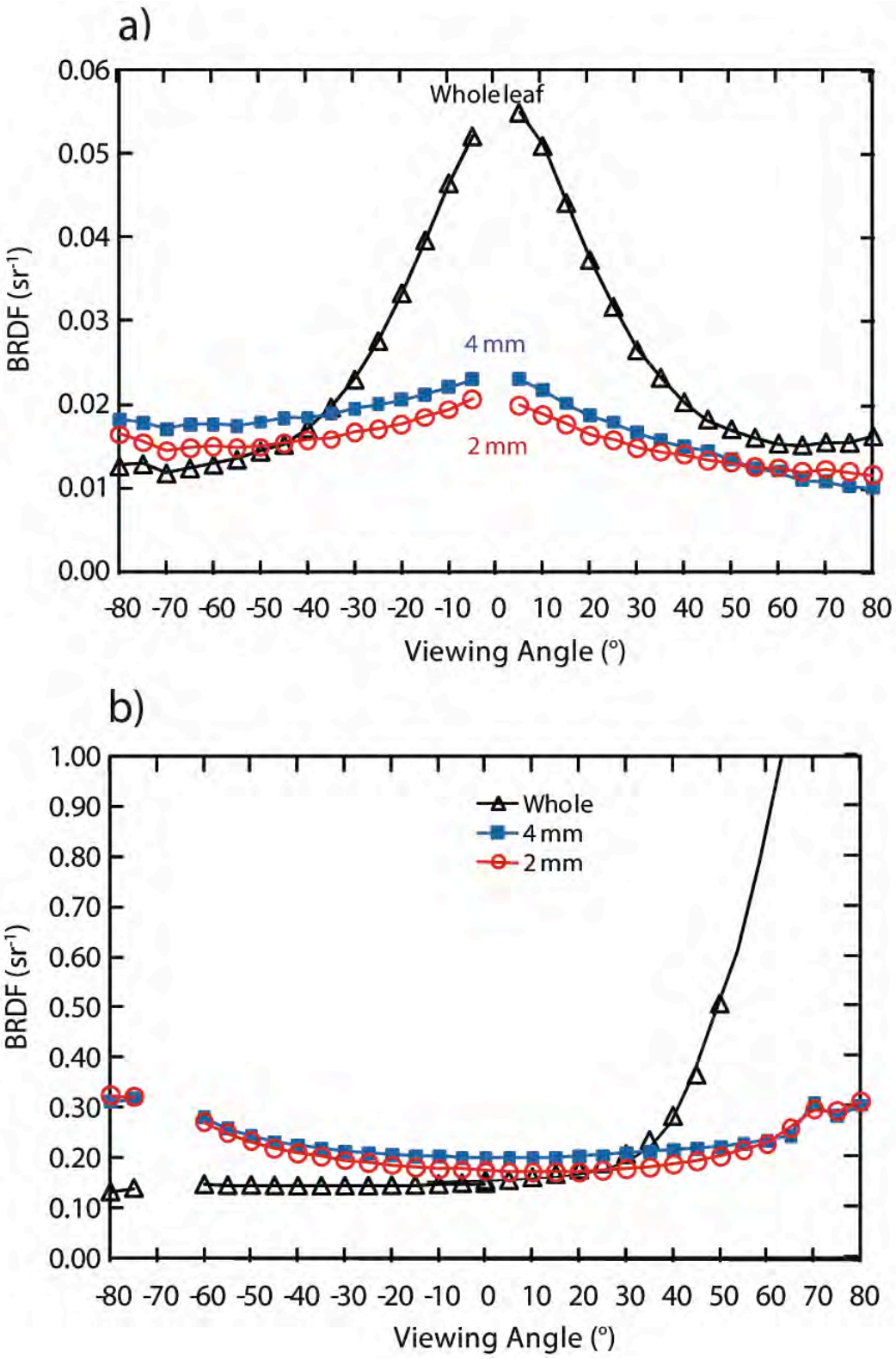

Fig. 7. BRDF of whole, 4 mm, and 2 mm cut poplar leaves at a) normal incidence and 340 nm. b) 67° incidence and 870 nm.

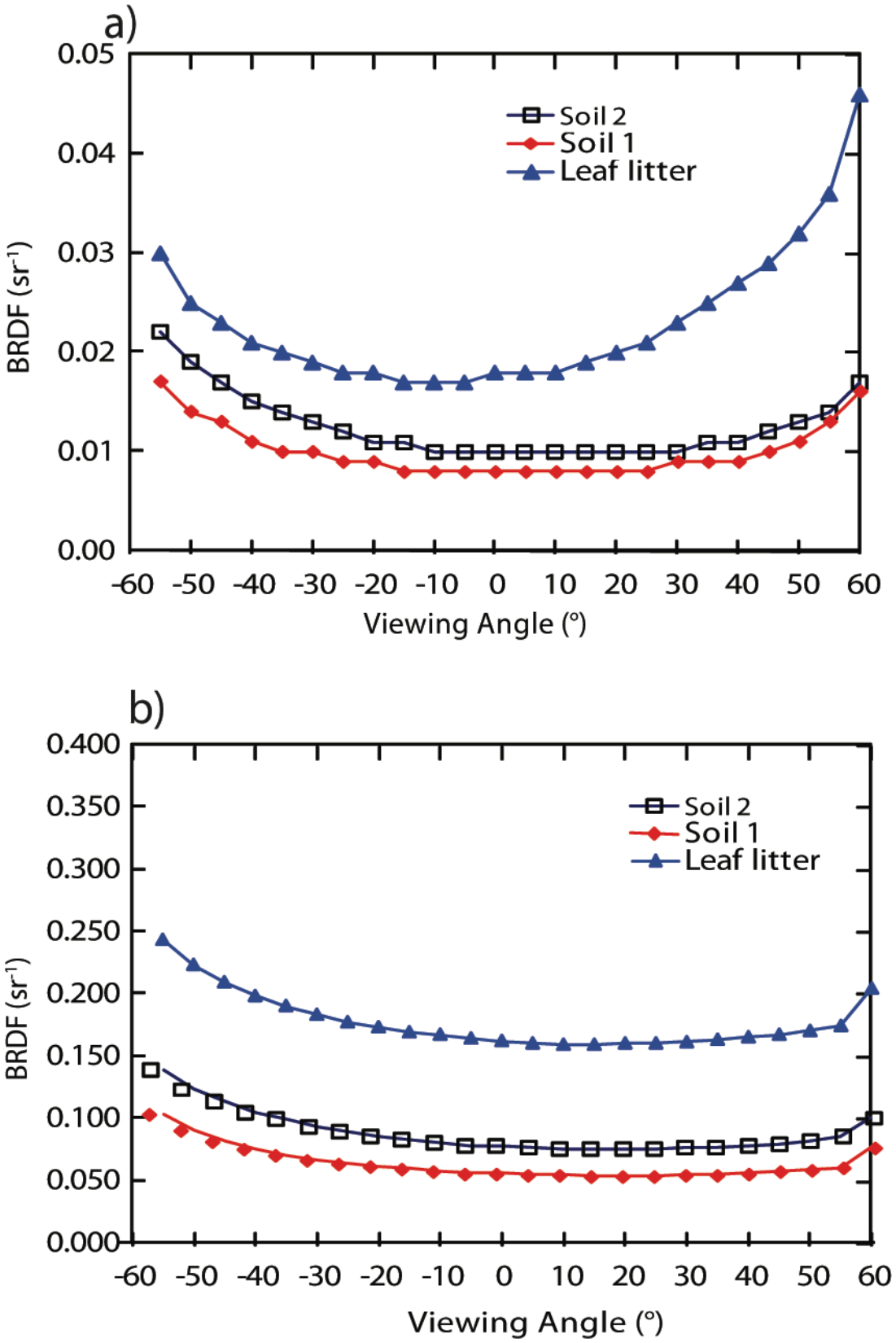

Fig. 8. BRDF of soil and leaf litter at 60° incidence; a) 340 nm, b) 870 nm

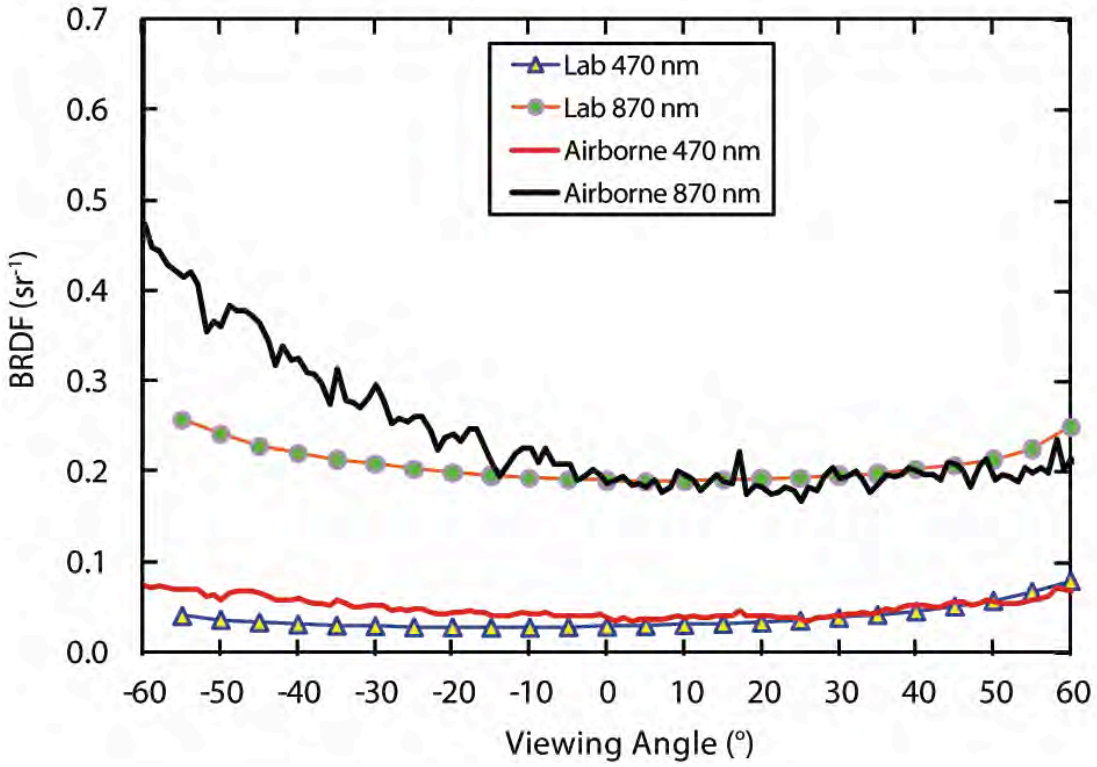

Fig. 9. Simulated scene BRDF from the fractional laboratory-based BRDF measurements and CAR airborne data at 470 and 870 nm.

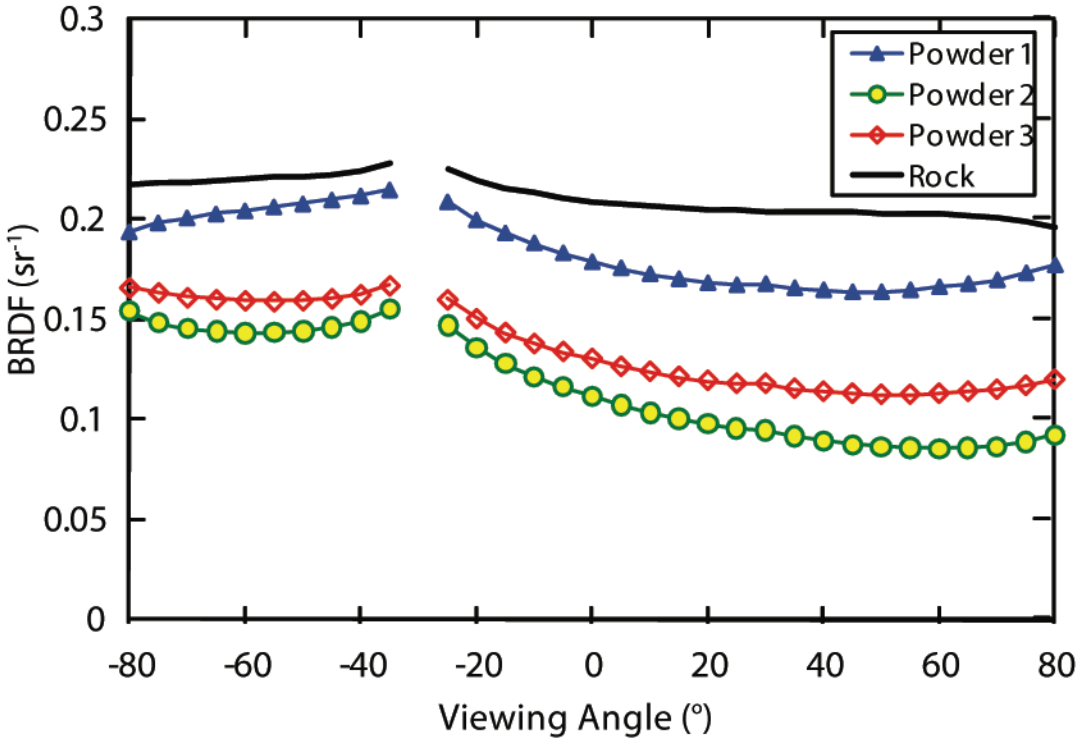

Fig. 10. BRDF of Etosha Pan samples at 30° incident angle and 667 nm.

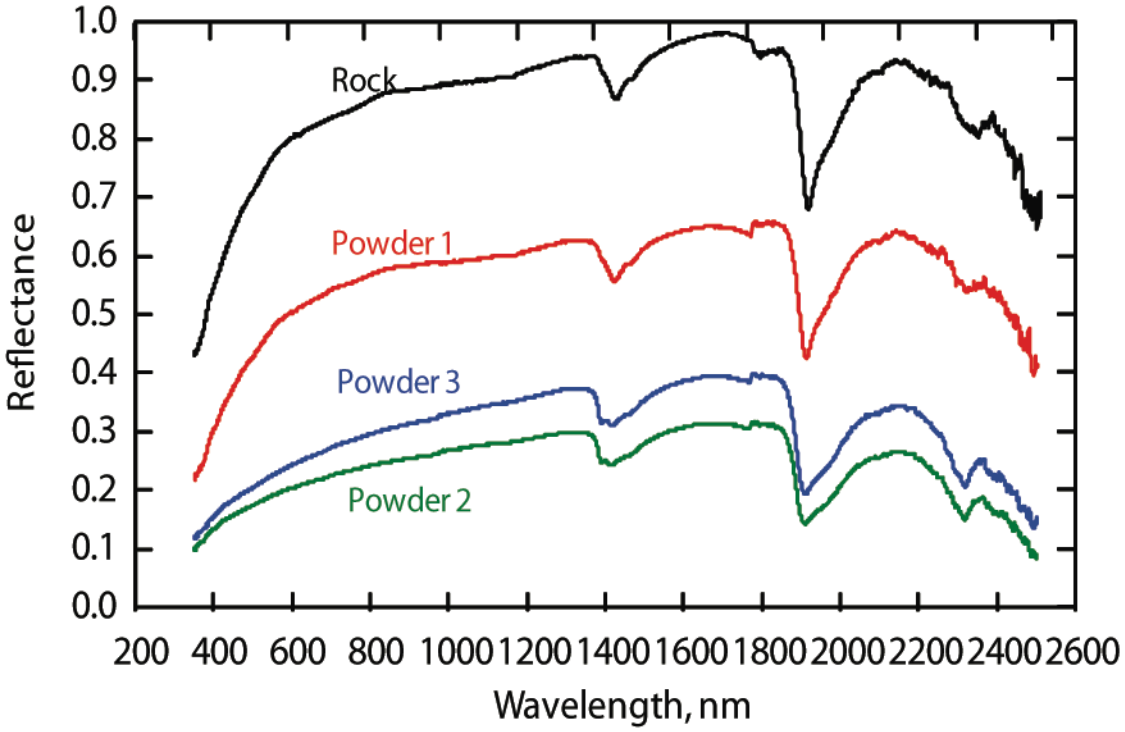

Fig. 11. ASD measured reflectance of Etosha Pan samples at 30^{o} incident angle and 30^{o} scatter zenith angle.

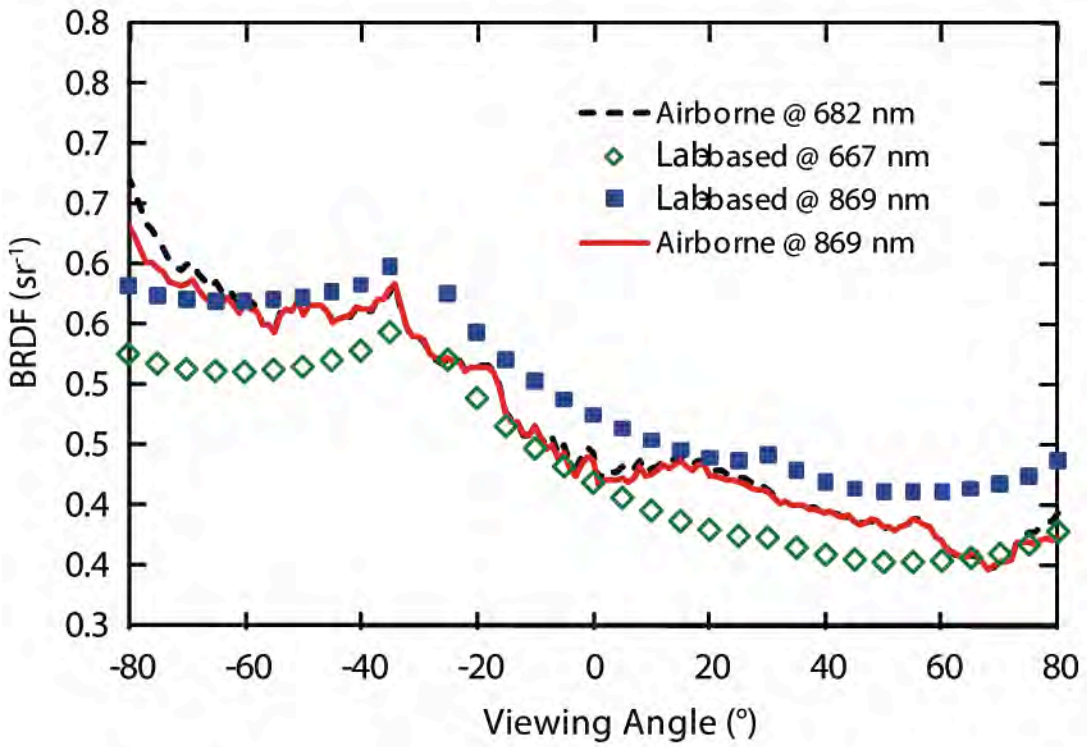

Fig. 12. Etosha Pan simulated scene BRDF from the fractional laboratory-based BRDF and CAR airborne data.